DETECTION PERFORMANCE OF RIS-AIDED MIMO RADAR WITH ASYNCHRONOUS PROPAGATION

Fangzhou Wang, A. Lee Swindlehurst*

Hongbin Li[†]

Center for Pervasive Comm. & Computing University of California Irvine Irvine, CA 92620, USA Dept. of Electrical & Computer Engr. Stevens Institute of Technology Hoboken, NJ 07030, USA

ABSTRACT

his paper explores the use of reconfigurable intelligent surfaces (RISs) for moving target detection in multi-input multi-output (MIMO) radar. Unlike previous related works that ignore the propagation delay difference between the direct path and the RIS-reflected path, we examine the detection problem in RIS-assisted MIMO radar by taking into account the effect of asynchronous propagation. Specifically, we first develop a general signal model for RIS-aided MIMO radar with multiple asynchronous RISs and arbitrary waveforms. Next, we formulate the RIS design problem by maximizing the overall received signal energy. The resulting optimization problem is non-convex, which is solved with semidefinite relaxation (SDR) techniques. A coherent detector is introduced for target detection. Finally, numerical results are presented to demonstrate the performance of the RIS-aided MIMO radar in comparison with the conventional MIMO radar.

Index Terms— Reconfigurable intelligent surfaces, MIMO radar, asynchronous propagation.

1. INTRODUCTION

Reconfigurable intelligent surfaces (RIS) are smart devices that enable realization of programmable RF propagation environments, and are emerging as a promising wireless technology for next generation systems [1–6]. Initially proposed for communication purposes, RISs have also recently received considerable attention within the radar community [7–11], as they can be leveraged to enhance target detection and localization performance [12–15]. The large number of degrees of freedom (DoFs) provided by an RIS also facilitates spectrum sharing between radar and communication systems [16–19].

Meanwhile, multi-input multi-output (MIMO) radar has been widely recognized as a vital radar technology with diverse applications [20,21]. A MIMO radar transmits multiple waveforms to probe the environment and at each receiver (RX), a set of matched filters (MFs), each matched to one of the transmitted waveforms, is employed to separate the information carried by different waveforms. The transmitted waveforms are frequently assumed to be orthogonal to each other with zero cross-correlation, such that the target echoes originating from different transmitters (TXs) can be separated by the MFs. However, it is infeasible to maintain strict orthogonality, in particular in distributed systems, where different propagation paths experience difference delays and Doppler shifts [22]. This has led to

several studies on MIMO radar with general non-orthogonal waveforms [23–25].

MIMO radar assisted by RIS has recently been considered in [12], covering both monostatic and bistatic radar configurations with or without a line-of-sight (LOS) view of the prospective target. The model therein assumes that different transmitters send distinct and orthogonal waveforms, which propagate through direct and RIS-reflected paths before synchronously arriving at the receiver. An RIS-aided radar is in general a distributed sensing system since the RIS is usually positioned separately from the radar transmitter and receiver locations to provide spatial diversity. Consequently, the target signal reflected by the RIS may reach the radar receiver at a different time compared with the direct path, and hence the RIS-reflected signal will be asynchronous.

In this paper, we consider moving target detection using a MIMO radar aided by multiple asynchronous RISs. Specifically, we first develop a general signal model for the considered system, assuming arbitrary non-orthogonal waveforms and asynchronous signal propagation. Then, the phase shifts of the RIS elements are designed by maximizing the overall received signal energy at the RX. Finally, the detection performance of the RIS-aided MIMO system is evaluated via numerical simulation and compared with a conventional MIMO radar.

2. SIGNAL MODEL

Consider a bistatic MIMO radar system with M closely spaced TXs and N closely spaced RXs, where the TXs employ pulsed transmission and a succession of K periodic pulses are transmitted during a coherent processing interval. Each transmit antenna emits a different baseband signal $u_m(t) = \sum_{k=0}^{K-1} p_m(t-kT_s)$, where $p_m(t)$ is the complex envelope of a single pulse for the m-th TX and T_s is the pulse repetition interval (PRI). Thus, at the m-th TX, the transmitted signal is given by $s_m(t) = u_m(t)e^{j2\pi f_c t}$, where f_c is the carrier frequency. The pulse waveform $p_m(t)$ has unit energy and is of a duration T_p .

To enhance the surveillance of an area of interest, L RISs, each consisting of Q reflecting elements, are deployed to assist the RX. Suppose there is a moving target at a distance $R_{\rm t}$ to the TX, a distance $R_{\rm t,\ell}$ to the ℓ -th RIS, and a distance $R_{\rm r}$ to the RX. The noise-free signal observed at the n-th RX can be expressed in complex-equivalent form as

$$\widetilde{s}_n(t) = \alpha \sum_{m=1}^{M} \left(\widetilde{\xi}_0 u_m(t - \tau_0) e^{j2\pi (f_c + f_0)(t - \tau_0)} a_m(\phi_{t,0}) \right)$$
 (1)

^{*}Supported by NSF grants CNS-2107182 and ECCS-2030029.

[†]Supported by NSF grants ECCS-1923739, ECCS-2212940, and CCF-2316865.

$$\times a_n(\phi_{\mathbf{r},0}) + \sum_{\ell=1}^L \widetilde{\xi}_{\ell} u_m(t - \tau_{\ell}) e^{\jmath 2\pi (f_c + f_{\ell})(t - \tau_{\ell})}$$

$$\times a_m(\phi_{\mathbf{t},0}) a_n(\phi_{\mathbf{r},\ell}) \sum_{q=1}^Q e^{\jmath \theta_{\ell,q}} a_q(\varphi_{\mathbf{r},\ell}) a_q(\varphi_{\mathbf{t},\ell}) \Big), \tag{2}$$

where α is the target radar cross section, τ_0 , ξ_0 , and f_0 are the propagation delay, the channel coefficient, and Doppler frequency for the TX-target-RX path, and τ_ℓ , $\widetilde{\xi}_\ell$, and f_ℓ are the corresponding parameters for the ℓ -th RIS. The variable $a_i(\phi)$ is the relative phase shift of the i-th array element, where ϕ is either the angle of departure (AoD) or angle of arrival (AoA) at the array. As an example, for a uniform linear array with elements separated by one half-wavelength, we have $a_i(\phi) = e^{-\jmath \pi (i-1)\sin\phi}$. The angles $\phi_{\rm t,0}, \phi_{\rm r,0}, \phi_{\rm r,\ell}$ respectively represent the AoD towards the target at the TX, the AoA at the RX due to the direct target reflection, and the AoA at the RX due to the signal reflected from the ℓ -th RIS. The angles $\varphi_{\rm r,\ell}$ and $\varphi_{\rm t,\ell}$ are the AoA and AoD at the ℓ -th RIS corresponding to the target reflected signal, respectively. The phase shift employed at the q-th element of the ℓ -th RIS is given by $e^{\jmath\theta_{\ell,q}}$.

After down conversion via a local carrier $e^{\jmath 2\pi f_c t}$, the baseband signal is

$$s_{n}(t) = \alpha \sum_{m=1}^{M} a_{m}(\phi_{t,0}) \left(\widetilde{\xi}_{0} u_{m}(t-\tau_{0}) e^{\jmath 2\pi f_{0}(t-\tau_{0})} e^{-\jmath 2\pi f_{c}\tau_{0}} \right)$$

$$\times a_{n}(\phi_{r,0}) + \sum_{\ell=1}^{L} \widetilde{\xi}_{\ell} u_{m}(t-\tau_{\ell}) e^{\jmath 2\pi f_{\ell}(t-\tau_{\ell})} e^{-\jmath 2\pi f_{c}\tau_{\ell}}$$

$$\times a_{n}(\phi_{r,\ell}) \sum_{q=1}^{Q} e^{\jmath \theta_{\ell,q}} a_{q}(\varphi_{r,\ell}) a_{q}(\varphi_{t,\ell}) \right).$$

$$(3)$$

Next, the baseband signal passes through a set of matched filters (MFs) matched to the radar waveforms along with delay and Doppler compensation. In particular, M MFs, i.e., $g_m(t)=p_m^*(-t)e^{\jmath 2\pi f_0t},$ $m=1,\cdots,M$, each matched to one of the M transmitted waveforms, are convolved with the received signal $s_n(t)$. Then, the output of the m-th MF at the n-th RX can be written as

$$\begin{split} x_{m,n}(t) &= \int s_n(\mu) g_m(t-\mu) d\mu = \int \left\{ \alpha \sum_{\bar{m}=1}^M a_{\bar{m}}(\phi_{\mathsf{t},0}) \right. \\ &\times \left(\widetilde{\xi}_0 \sum_{k=0}^{K-1} p_{\bar{m}}(\mu - kT_\mathsf{s} - \tau_0) e^{\jmath 2\pi f_0(\mu - \tau_0)} e^{-\jmath 2\pi f_c \tau_0} a_n(\phi_{\mathsf{r},0}) \right. \\ &+ \sum_{\ell=1}^L \widetilde{\xi}_\ell \sum_{k=0}^{K-1} p_{\bar{m}}(\mu - kT_\mathsf{s} - \tau_\ell) e^{\jmath 2\pi f_\ell(\mu - \tau_\ell)} e^{-\jmath 2\pi f_c \tau_\ell} a_n(\phi_{\mathsf{r},\ell}) \\ &\times \sum_{q=1}^Q e^{\jmath \theta_{\ell,q}} a_q(\varphi_{\mathsf{r},\ell}) a_q(\varphi_{\mathsf{t},\ell}) \right\} p_m^*(\mu - t) e^{\jmath 2\pi f_0(t-\mu)} d\mu \\ &= \alpha \sum_{\bar{m}=1}^M a_{\bar{m}}(\phi_{\mathsf{t},0}) \left(\widetilde{\xi}_0 e^{-\jmath 2\pi f_c \tau_0} e^{\jmath 2\pi f_0(t-\tau_0)} a_n(\phi_{\mathsf{r},0}) \right. \\ &\times \sum_{k=0}^{K-1} \chi_{m,\bar{m}}(t-kT_\mathsf{s} - \tau_0,0) \\ &+ \sum_{k=0}^L \widetilde{\xi}_\ell e^{-\jmath 2\pi f_c \tau_\ell} e^{\jmath 2\pi f_0(t-\tau_\ell)} a_n(\phi_{\mathsf{r},\ell}) \sum_{k=0}^{K-1} e^{\jmath 2\pi kT_\mathsf{s}(f_\ell - f_0)} \end{split}$$

$$\times \chi_{m,\bar{m}}(t - kT_{\rm s} - \tau_{\ell}, f_{\ell} - f_0) \sum_{q=1}^{Q} e^{j\theta_{\ell,q}} a_q(\varphi_{\rm r,\ell}) a_q(\varphi_{\rm t,\ell}) \Big), \tag{4}$$

where the ambiguity function $\chi_{m,\bar{m}}(\bar{\tau},\bar{f})$ is defined as

$$\chi_{m,\bar{m}}(\bar{\tau},\bar{f}) \triangleq \int p_{\bar{m}}(\mu) p_m^*(\mu - \bar{\tau}) e^{\jmath 2\pi \bar{f}\mu} d\mu. \tag{5}$$

The continuous-time signal $x_{m,n}(t)$ is sampled at the pulse rate, leading to K slow-time samples obtained at time instants $t=\tau_0+kT_s,\ k=0,\cdots,K-1$, which yields the discrete-time received signal

$$x_{m,n}(k) = x_{m,n}(t) \Big|_{t=\tau_0 + kT_s}$$

$$= \alpha \sum_{\bar{m}=1}^{M} a_{\bar{m}}(\phi_{t,0}) \Big(\tilde{\xi}_0 e^{-j2\pi f_c \tau_0} e^{j2\pi kT_s f_0} a_n(\phi_{r,0}) \chi_{m,\bar{m}}(0,0)$$

$$+ \sum_{\ell=1}^{L} \tilde{\xi}_{\ell} e^{-j2\pi f_c \tau_{\ell}} e^{j2\pi f_0(\tau_0 - \tau_{\ell})} a_n(\phi_{r,\ell}) e^{j2\pi kT_s f_{\ell}}$$

$$\times \chi_{m,\bar{m}}(\tau_0 - \tau_{\ell}, f_{\ell} - f_0) \sum_{\ell=1}^{Q} e^{j\theta_{\ell,q}} a_q(\varphi_{r,\ell}) a_q(\varphi_{t,\ell}) \Big).$$
 (6)

Next, we stack the K slow-time samples and form $\mathbf{x}_{m,n} = [x_{m,n}(0), \cdots, x_{m,n}(K-1)]^T$, which can be expressed as

$$\mathbf{x}_{m,n} = \alpha \xi_{n,0} h_{m,0} \mathbf{s}(f_0) + \alpha \sum_{\ell=1}^{L} \xi_{n,\ell} h_{m,\ell} \beta_{\ell} \mathbf{s}(f_{\ell}), \qquad (7)$$

where

- $h_{m,\ell}=e^{-j2\pi f_c\tau_\ell}e^{j2\pi f_0(\tau_0-\tau_\ell)}\sum_{\bar{m}=1}^M\chi_{m,\bar{m}}(\tau_0-\tau_\ell,f_\ell-f_0)a_{\bar{m}}(\phi_{\rm t,0})$ and $\xi_{n,\ell}=\widetilde{\xi}_\ell a_n(\phi_{\rm r,\ell})$ for $\ell=0,1,\cdots,L$. Note that for $\ell=0$, i.e., $h_{m,0}$ and $\xi_{n,0}$, are the channel coefficients corresponding to the direct path from the TX to the target and then to the RX (denoted as the direct-propagation path in the rest of the paper) while $h_{m,\ell}$ and $\xi_{n,\ell}$ when $\ell\neq 0$ are the channel coefficients of the RIS-assisted indirect paths.
- $\mathbf{s}(f)=[1,e^{\jmath 2\pi T_{\rm s}f},\cdots,e^{\jmath 2\pi(K-1)T_{\rm s}f}]^T$ is the Doppler steering vector.
- $\beta_{\ell} = \sum_{q=1}^{Q} e^{j\theta_{\ell,q}} a_q(\varphi_{\mathbf{r},\ell}) a_q(\varphi_{\mathbf{t},\ell})$ for $\ell = 1, \dots, L$ is the overall phase shift at the ℓ -th RIS.

Note that the output sample $x_{m,n}(k)$ consists of L+1 terms, the first of which is due to the direct path, while the remaining L terms are the RIS-assisted paths. In addition, it can be seen that all of the channel coefficients $h_{m,0}$ and $h_{m,\ell}$ have M components, i.e., the auto-correlation term, which is the MF output matched to the desired waveform (e.g., $m = \bar{m}$), and M - 1 cross terms, which are filtered echoes from the undesired waveforms (e.g., $m \neq \bar{m}$). The auto- and cross-correlation terms may add constructively or destructively depending on their relative phases. Under the condition that the waveforms are orthogonal across all delays and Dopplers of interest with zero cross-correlation, a frequently used assumption in the literature, the coefficients contain only the auto- and none of the cross-correlation terms, which results in ideal waveform separation, i.e., $\chi_{m,\bar{m}}(\tau_0 - \tau_\ell, f_\ell - f_0) = 0$ when $m \neq \bar{m}$. However, such strict orthogonality is infeasible in practice. Moreover, even with ideal orthogonal waveforms, the auto-correlation terms for the RIS-assisted paths are sampled off the peak location of the auto ambiguity function, i.e., $\chi_{m,m}(\tau_0 - \tau_\ell, f_\ell - f_0)$ for $\tau_0 \neq \tau_\ell$ and $f_\ell \neq f_0$. This means there could be considerable energy loss for the RIS-assisted paths due to asynchronous propagation.

3. PROPOSED METHODS

3.1. RIS Design

The problem of interest is to design the RIS phase shifts $e^{j\theta_{\ell,q}}$ by maximizing the received signal energy, i.e.,

$$\max_{\{\theta_{\ell,q}\}} \sum_{m=1}^{M} \sum_{n=1}^{N} \|\mathbf{x}_{m,n}\|^{2}, \tag{8}$$

where the scaling factor $|\alpha|^2$ is ignored in the cost function since it does not affect the optimum solution of the optimization problem.

To solve the above nonlinear problem, we first rewrite the problem in a constrained optimization form. Specifically, define

$$\boldsymbol{\phi}_{\ell} \triangleq \left[e^{\jmath \theta_{\ell,1}}, \cdots, e^{\jmath \theta_{\ell,Q}} \right]^{T},$$
 (9a)

$$\phi \triangleq [\phi_1^T, \cdots, \phi_L^T]^T, \tag{9b}$$

$$\mathbf{a}_{\ell} \triangleq \left[a_1(\varphi_{\mathsf{r},\ell}) a_1(\varphi_{\mathsf{t},\ell}), \cdots, a_Q(\varphi_{\mathsf{r},\ell}) a_Q(\varphi_{\mathsf{t},\ell}) \right]^T, \qquad (9c)$$

$$\mathbf{d}_{m,n} \triangleq \xi_{n,0} h_{m,0} \mathbf{s}(f_0), \tag{9d}$$

$$\widetilde{\mathbf{d}}_{m,n,\ell} \triangleq \xi_{n,\ell} h_{m,\ell} \mathbf{s}(f_{\ell}).$$
 (9e)

Then the optimization problem (7) becomes

$$\max_{\phi} \sum_{m=1}^{M} \sum_{n=1}^{N} \|\mathbf{d}_{m,n} + \mathbf{D}_{m,n} \phi\|^{2}$$
 (10a)

$$s.t. |\phi| = 1, \tag{10b}$$

ulus constraint (9b). It can be recast as a unit-modulus constrained quadratic program and solved by the semidefinite relaxation (SDR) technique.

Letting $\widetilde{\phi} = [\phi^T, 1]^T$, the non-homogeneous quadratic cost function in (9) can be converted to

$$\|\mathbf{d}_{m,n} + \mathbf{D}_{m,n}\boldsymbol{\phi}\|^2 = \widetilde{\boldsymbol{\phi}}^H \mathbf{F}_{m,n} \widetilde{\boldsymbol{\phi}}, \tag{11}$$

where $\mathbf{F}_{m,n}$ is a $(QL+1)\times (QL+1)$ matrix given by

$$\mathbf{F}_{m,n} = \begin{bmatrix} \mathbf{D}_{m,n}^H \mathbf{D}_{m,n} & \mathbf{D}_{m,n}^H \mathbf{d}_{m,n} \\ \mathbf{d}_{m,n}^H \mathbf{D}_{m,n} & \mathbf{d}_{m,n}^H \mathbf{d}_{m,n} \end{bmatrix}. \tag{12}$$

Thus, let $\mathbf{F} = \sum_{m=1}^{M} \sum_{n=1}^{N} \mathbf{F}_{m,n}$. The optimization problem in (9) can be rewritten as

$$\max_{\widetilde{\phi}} \ \widetilde{\phi} \mathbf{F} \widetilde{\phi} \tag{13a}$$
 s.t. $|\widetilde{\phi}| = 1, \ \widetilde{\phi}(QL + 1) = 1. \tag{13b}$

s.t.
$$|\widetilde{\phi}| = 1$$
, $\widetilde{\phi}(QL + 1) = 1$. (13b)

In the following, we apply SDR to convert (12) into a convex problem by dropping the rank-one constraint. Specifically, let $\Phi = \widetilde{\phi} \widetilde{\phi}^H$ so that the SDR form of problem (12) becomes

$$\max_{\mathbf{F}} \operatorname{tr}(\mathbf{\Phi}\mathbf{F}) \tag{14a}$$

s.t.
$$|\Phi(i, i)| = 1, i = 1, \dots, QL + 1,$$
 (14b)

which is a convex problem and can be solved by CVX [26].

The optimum SDR solution $\hat{\Phi}$ to (13) needs to be converted into a feasible solution ϕ to (12), which can be achieved through a randomization appraoch [27]. Specifically, given the optimum $\hat{\Phi}$, a

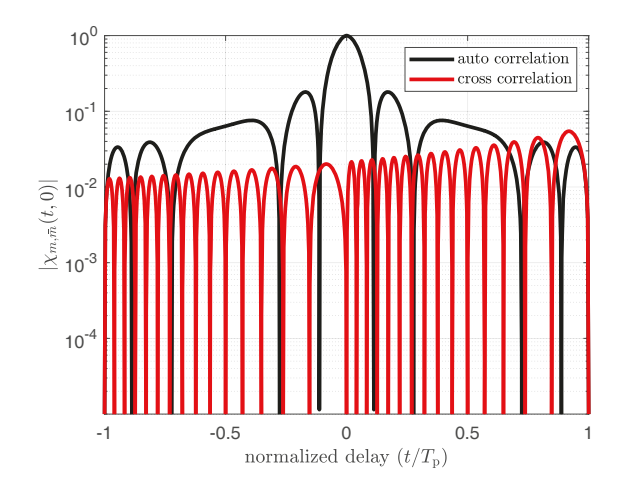


Fig. 1. Waveform ambiguity function when $\beta = 1$ MHz.

set of Gaussian random vectors are generated, i.e., $\boldsymbol{\xi}_i \sim \mathcal{CN}(\mathbf{0}, \hat{\boldsymbol{\Phi}})$, $j=1,\cdots,J$, where J is the number of random trials. Note that the random vectors $\boldsymbol{\xi}_i$ do not always satisfy the unit-modulus constraint and the constraint $\widetilde{\phi}(QL+1)=1$ in (12). Thus, we need to first normalize them as $\bar{\boldsymbol{\xi}}_j = \boldsymbol{\xi}_j/\boldsymbol{\xi}_j(QL+1)$ to satisfy the constraint $\widetilde{\phi}(QL+1)=1$. Then, to meet the constraint $|\widetilde{\phi}|=1$, the feasible solution can be further recovered by $\hat{\xi}_j(i)=e^{\jmath\angle(\overline{\xi}_j(i))}$ for i=1where $\mathbf{D}_{m,n}$ is a $K \times QL$ matrix defined as $\mathbf{D}_{m,n} = [\widetilde{\mathbf{d}}_{m,n,1}\mathbf{a}_1^T, \cdots, \widetilde{\mathbf{d}}_{m,n,L}^T \widetilde{\mathbf{d}}_L^T QL$. Finally, the rank-one solution can be obtained as $\hat{\boldsymbol{\phi}} = \mathbf{D}_{m,n}$ are $\mathbf{d}_{m,n} = \mathbf{d}_{m,n} = \mathbf{d}_$

3.2. Target Detection

For target detection we employ a coherent detector, which can be derived using a generalized likelihood ratio test framework, similarly to [25]:

$$T = \left| \sum_{m=1}^{M} \sum_{n=1}^{N} \mathbf{b}_{m,n}^{H} \mathbf{y}_{m,n} \right|^{2} \underset{\mathcal{H}_{0}}{\gtrless} \gamma, \tag{15}$$

where γ denotes the threshold and $\mathbf{b}_{m,n}$ is a weighted sum of the channel coefficients and Doppler steering vector [cf. (6)]

$$\mathbf{b}_{m,n} = \xi_{n,0} h_{m,0} \mathbf{s}(f_0) + \sum_{\ell=1}^{L} \xi_{n,\ell} h_{m,\ell} \beta_{\ell} \mathbf{s}(f_{\ell}).$$
 (16)

4. NUMERICAL RESULTS

In this section, simulation results are presented to demonstrate the performance of the RIS-aided MIMO radar system. The signal-tonoise ratio (SNR) is defined as SNR = $\frac{\mathbb{E}\{|\alpha|^2\}}{\sigma^2}$, where the noise variance is chosen as $\sigma^2 = 1$. The target RCS is randomly generated as $\alpha \sim \mathcal{CN}(0, \sigma_0^2)$, where σ_0^2 is determined based on the specific SNR.

In the simulations, linear frequency modulation (LFM) based waveforms, also known as chirps, are employed as test waveforms. Specifically, a set of multi-band chirps are utilized [28]:

$$p_m(t) = \frac{1}{\sqrt{T_p}} e^{j\pi\beta(t^2/T_p + \eta m t)}, 0 \le t \le T_p,$$
 (17)

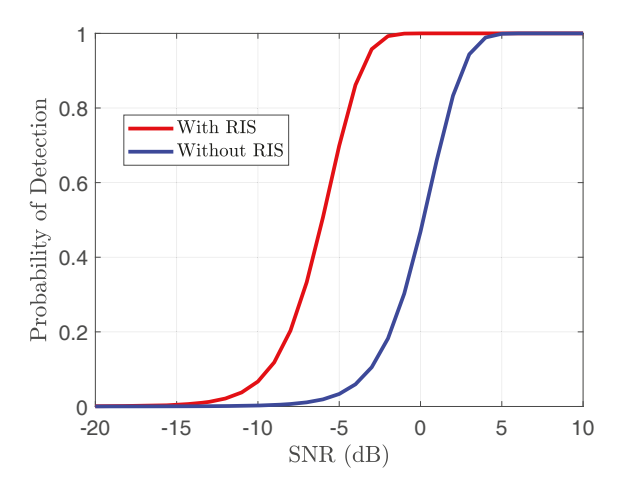


Fig. 2. Probability of detection versus SNR.

where β is the bandwidth of the waveform and η is a bandwidth gap parameter that is selected to keep the frequency bands of different waveforms from overlapping. Fig. 1 shows the ambiguity functions defined in (4) when using the chirp in (16) for $M=3, \eta=3$, and $\beta=1$ MHz. It can be observed that the multi-band chirps are approximately orthogonal with low autocorrelation sidelobes and low cross-correlation levels. The non-zero cross-correlation is caused by leakage.

We consider a co-located MIMO radar system with $M=3\,\mathrm{TXs}$ and $N=3\,\mathrm{RXs}$. The TX is located at $(0,\,0)\mathrm{m}$ and the RX is located at $(400,\,0)\mathrm{m}$. Unless otherwise stated, there are two RISs located at $(350,\,100)\mathrm{m}$ and $(200,\,-50)\mathrm{m}$, respectively. The number of elements in each RIS is Q=64. The carrier frequency is $f_c=3$ GHz, the pulse duration is $T_p=10^{-5}\mathrm{s}$, and the pulse repetition frequency (PRF) is 500 Hz. The target velocity is 30 m/s and the target is located at $[100,\,200]\,\mathrm{m}$. The number of pulses within a CPI is K=12 unless otherwise stated and the probability of false alarm is $P_f=10^{-4}$.

The performance of a conventional MIMO radar system without an RIS is included as a benchmark for comparison. Fig. 2 depicts the probability of detection versus SNR. It can be observed that the RIS-aided MIMO radar system outperforms the conventional MIMO radar without RIS. This is because the MF output (6) contains L+1 terms and the RIS propagation related terms are also non-zero and can provide additional energy for target detection, which is not possible for the scenario without RIS.

Next, we evaluate the impact of the RIS location on the target detection performance. Fig. 3 shows the performance of the RIS-aided MIMO radar system for various RIS locations, where a single RIS is deployed either near the radar RX at (400, 10)m or far away from the radar RX at (400, 150)m. It can be observed from Fig 3 that the RIS-aided MIMO system outperforms the MIMO system without RIS for both RIS locations. The benefit of the RIS is more significant when it is deployed close to the radar RX. There are two reasons for this. First, when the RIS is deployed closer to the RX, the delay offset between the direct path propagation and the RIS-assisted path is smaller, which means the waveform ambiguity functions can be sampled closer to the peak value. Second, when the RIS is deployed far away from the RX, this leads to longer propagation distances, which in turn causes bigger attenuation and a weaker RIS-assisted channel strength.

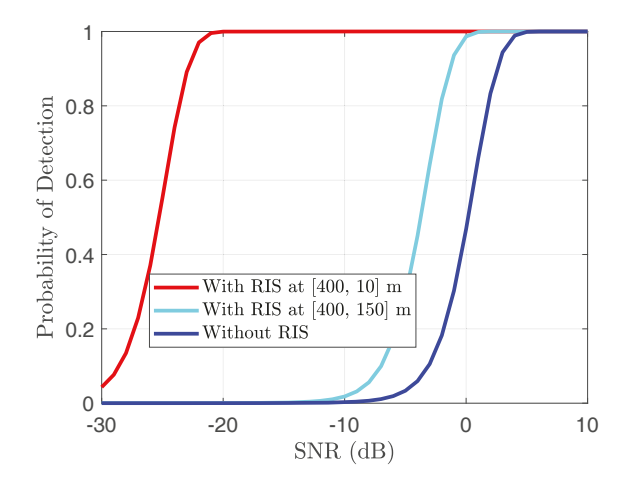


Fig. 3. Probability of detection versus SNR under various RIS deployment locations.

5. CONCLUSION

We developed a general signal model to account for asynchronous propagation in RIS-aided MIMO radar systems. An RIS phase shift design problem was formulated that maximizes the received signal energy, and an SDR approach was proposed to solve the problem. We studied the impact of the non-negligible propagation delay between the direct path and the RIS-reflected path on the target detection performance. Our results indicate that the propagation delay difference needs to be accounted for to benefit from the ability of the RIS to improve target detection performance.

6. REFERENCES

- [1] Chongwen Huang, Alessio Zappone, George C. Alexandropoulos, Mrouane Debbah, and Chau Yuen, "Reconfigurable intelligent surfaces for energy efficiency in wireless communication," *IEEE Transactions on Wireless Communications*, vol. 18, no. 8, pp. 4157–4170, 2019.
- [2] Peilan Wang, Jun Fang, Xiaojun Yuan, Zhi Chen, and Hongbin Li, "Intelligent reflecting surface-assisted millimeter wave communications: Joint active and passive precoding design," *IEEE Transactions on Vehicular Technology*, vol. 69, no. 12, pp. 14960–14973, 2020.
- [3] Cunhua Pan, Hong Ren, Kezhi Wang, Jonas Florentin Kolb, Maged Elkashlan, Ming Chen, Marco Di Renzo, Yang Hao, Jiangzhou Wang, A. Lee Swindlehurst, Xiaohu You, and Lajos Hanzo, "Reconfigurable intelligent surfaces for 6G systems: Principles, applications, and research directions," *IEEE Communications Magazine*, vol. 59, no. 6, pp. 14–20, 2021.
- [4] Zijian Zhang, Linglong Dai, Xibi Chen, Changhao Liu, Fan Yang, Robert Schober, and H. Vincent Poor, "Active RIS vs. passive RIS: Which will prevail in 6G?," *IEEE Transactions* on Communications, vol. 71, no. 3, pp. 1707–1725, 2023.
- [5] Rang Liu, Ming Li, Honghao Luo, Qian Liu, and A. Lee Swindlehurst, "Integrated sensing and communication with reconfigurable intelligent surfaces: Opportunities, applications, and future directions," *IEEE Wireless Communications*, vol. 30, no. 1, pp. 50–57, 2023.

- [6] Fangzhou Wang and A. Lee Swindlehurst, "Hybrid ris-assisted interference mitigation for spectrum sharing," in *ICASSP 2023 2023 IEEE International Conference on Acoustics, Speech and Signal Processing (ICASSP)*, 2023, pp. 1–5.
- [7] R. S. Prasobh Sankar, Battu Deepak, and Sundeep Prabhakar Chepuri, "Joint communication and radar sensing with reconfigurable intelligent surfaces," in 2021 IEEE 22nd International Workshop on Signal Processing Advances in Wireless Communications (SPAWC), 2021, pp. 471–475.
- [8] Augusto Aubry, Antonio De Maio, and Massimo Rosamilia, "Reconfigurable intelligent surfaces for N-LOS radar surveillance," *IEEE Transactions on Vehicular Technology*, vol. 70, no. 10, pp. 10735–10749, 2021.
- [9] Zahra Esmaeilbeig, Kumar Vijay Mishra, and Mojtaba Soltanalian, "IRS-aided radar: Enhanced target parameter estimation via intelligent reflecting surfaces," in 2022 IEEE 12th Sensor Array and Multichannel Signal Processing Workshop (SAM), 2022, pp. 286–290.
- [10] Fangzhou Wang, Hongbin Li, and Jun Fang, "Joint active and passive beamforming for IRS-assisted radar," *IEEE Sig*nal Processing Letters, vol. 29, pp. 349–353, 2022.
- [11] Fangzhou Wang, Hongbin Li, and A. Lee Swindlehurst, "Clutter suppression for target detection using hybrid reconfigurable intelligent surfaces," in 2023 IEEE Radar Conference (Radar-Conf23), 2023, pp. 1–5.
- [12] Stefano Buzzi, Emanuele Grossi, Marco Lops, and Luca Venturino, "Foundations of MIMO radar detection aided by reconfigurable intelligent surfaces," *IEEE Transactions on Signal Processing*, vol. 70, pp. 1749–1763, 2022.
- [13] Kamran Keykhosravi, Musa Furkan Keskin, Gonzalo Seco-Granados, Petar Popovski, and Henk Wymeersch, "Risenabled siso localization under user mobility and spatial-wideband effects," *IEEE Journal of Selected Topics in Signal Processing*, vol. 16, no. 5, pp. 1125–1140, 2022.
- [14] Alessio Fascista, Musa Furkan Keskin, Angelo Coluccia, Henk Wymeersch, and Gonzalo Seco-Granados, "RIS-aided joint localization and synchronization with a single-antenna receiver: Beamforming design and low-complexity estimation," *IEEE Journal of Selected Topics in Signal Processing*, vol. 16, no. 5, pp. 1141–1156, 2022.
- [15] Reza Ghazalian, Hui Chen, George C. Alexandropoulos, Gonzalo Seco-Granados, Henk Wymeersch, and Riku Jntti, "Joint user localization and location calibration of a hybrid reconfigurable intelligent surface," 2022.
- [16] Rang Liu, Ming Li, Yang Liu, Qingqing Wu, and Qian Liu, "Joint transmit waveform and passive beamforming design for RIS-aided DFRC systems," *IEEE Journal of Selected Topics* in Signal Processing, vol. 16, no. 5, pp. 995–1010, 2022.
- [17] Yikai Li and Athina Petropulu, "Dual-function radar-communication system aided by intelligent reflecting surfaces," in 2022 IEEE 12th Sensor Array and Multichannel Signal Processing Workshop (SAM), 2022, pp. 126–130.
- [18] Tong Wei, Linlong Wu, Kumar Vijay Mishra, and M. R. Bhavani Shankar, "IRS-aided wideband dual-function radar-communications with quantized phase-shifts," in 2022 IEEE 12th Sensor Array and Multichannel Signal Processing Workshop (SAM), 2022, pp. 465–469.

- [19] Fangzhou Wang and A. Lee Swindlehurst, "Applications of absorptive reconfigurable intelligent surfaces in interference mitigation and physical layer security," 2023.
- [20] Jian Li and Petre Stoica, "MIMO radar with colocated antennas," *IEEE Signal Processing Magazine*, vol. 24, no. 5, pp. 106–114, 2007.
- [21] Alexander M. Haimovich, Rick S. Blum, and Leonard J. Cimini, "MIMO radar with widely separated antennas," *IEEE Signal Processing Magazine*, vol. 25, no. 1, pp. 116–129, 2008.
- [22] Yuri I. Abramovich and Gordon J. Frazer, "Bounds on the volume and height distributions for the MIMO radar ambiguity function," *IEEE Signal Processing Letters*, vol. 15, pp. 505– 508, 2008.
- [23] Murat Akcakaya and Arye Nehorai, "MIMO radar sensitivity analysis for target detection," *IEEE Transactions on Signal Processing*, vol. 59, no. 7, pp. 3241–3250, 2011.
- [24] Pu Wang and Hongbin Li, "Target detection with imperfect waveform separation in distributed MIMO radar," *IEEE Trans*actions on Signal Processing, vol. 68, pp. 793–807, 2020.
- [25] Hongbin Li, Fangzhou Wang, Cengcang Zeng, and Mark A. Govoni, "Signal detection in distributed MIMO radar with non-orthogonal waveforms and sync errors," *IEEE Transac*tions on Signal Processing, vol. 69, pp. 3671–3684, 2021.
- [26] Michael Grant and Stephen Boyd, "CVX: Matlab software for disciplined convex programming, version 2.1," http:// cvxr.com/cvx, Mar. 2014.
- [27] Zhi-Quan Luo, Wing-Kin Ma, Anthony Man-Cho So, Yinyu Ye, and Shuzhong Zhang, "Semidefinite relaxation of quadratic optimization problems," *IEEE Signal Processing Magazine*, vol. 27, no. 3, pp. 20–34, 2010.
- [28] Fangzhou Wang, Cengcang Zeng, Hongbin Li, and Mark A. Govoni, "Detection performance of distributed MIMO radar with asynchronous propagation and timing/phase errors," in 2020 IEEE International Radar Conference (RADAR), 2020, pp. 13–18.